HHS Public Access

Author manuscript

J Magn Reson Imaging. Author manuscript; available in PMC 2020 August 01.

Published in final edited form as:

J Magn Reson Imaging. 2019 August ; 50(2): 456–464. doi:10.1002/jmri.26636.

Machine learning-based prediction of future breast cancer using algorithmically measured background parenchymal enhancement on high-risk screening MRI

Ashirbani Saha[1], **Lars J. Grimm**[1], **Sujata V. Ghate**[1], **Connie E. Kim**[1], **Mary S. Soo**[1], **Sora C. Yoon**[1], and **Maciej A. Mazurowski**[1,2,3]

Ashirbani Saha: ashirbani.saha@duke.edu; Lars J. Grimm: lars.grimm@duke.edu; Sujata V. Ghate: sujata.ghate@duke.edu; Connie E. Kim: connie.kim@duke.edu; Mary S. Soo: mary.soo@duke.edu; Sora C. Yoon: sora.yoon@duke.edu; Maciej A. Mazurowski: maciej.mazurowski@duke.edu

[1]Department of Radiology, Duke University School of Medicine, Durham, NC 27710, USA

[2]Department of Electrical and Computer Eng., Duke University, Durham, NC 27708 USA

[3]Duke University Medical Physics Program, Durham, NC 27705, USA

Abstract

Background: Preliminary work has demonstrated that background parenchymal enhancement (BPE) assessed by radiologists is predictive of future breast cancer in women undergoing high-risk screening MRI. Algorithmically assessed measures of BPE offer a more precise and reproducible means of measuring BPE than human readers and thus might improve the predictive performance of future cancer development.

Purpose: To determine if algorithmically-extracted imaging features of background parenchymal enhancement (BPE) on screening breast MRI in high-risk women are associated with subsequent development of cancer.

Study Type: Case control study

Population: 133 women at high-risk for developing breast cancer. 46 of these patients developed breast cancer subsequently over a follow-up period of two years.

Field Strength/sequence: 1.5T or 3.0T T1-weighted pre-contrast fat saturated and non- fat saturated sequences and post contrast non-fat saturated sequences.

Assessment: Automatic features of BPE were extracted by computer algorithm. Subjective BPE scores from five breast radiologists (blinded to clinical outcomes) were also available.

Statistical Tests: Leave-one-out cross validation for a multivariate logistic regression model developed using the automatic features and receiver operating characteristic (ROC) analysis were performed to calculate the area-under-the-curve (AUC). Comparison of automatic features and subjective features was performed using a generalized regression model and p-value was obtained. Odds ratios for automatic and subjective features were compared.

Corresponding Author: Maciej A. Mazurowski, Ph.D., 2424 Erwin Road, Suite 302, Durham NC 27705 USA, Telephone: +1 (919) 684 1466, Fax: 919-684-1491, maciej.mazurowski@duke.edu.

Results: The multivariate model discriminated patients that developed cancer from the patients that did not with an AUC of 0.70 (95% CI: 0.60–0.79, p <0.001). The imaging features remained independently predictive of subsequent development of cancer (p <0.003) when compared to the subjective BPE assessment of the readers.

Data Conclusion: Automatically extracted BPE measurements may potentially be used to further stratify risk in patients undergoing high-risk screening MRI.

Keywords

high-risk breast cancer patients; background parenchymal enhancement; breast mask; vessel segmentation; breast MRI; high-risk screening

INTRODUCTION:

For women, breast cancer is the most common form of cancer and the second most common cause of breast cancer-related deaths (1). However, death rates in breast cancer have decreased by 36% over the past two decades, presumably due to early detection and treatment (1). For early detection, the American College of Radiology guidelines recommend screening mammography and MRI for high-risk patients (2). High-risk patients have more than 20% lifetime risk of developing breast cancer and breast cancer survival in these women is improved with combined MRI and mammography screening (3).

Though the aim of screening MRI is early detection of breast cancer, preliminary work has demonstrated that subjective radiologist measures of background parenchymal enhancement (BPE) can predict future cancer risk (4)(5). BPE is the enhancement of normal breast parenchyma which increases with hormonal activity and decreases with age(6). Increased BPE, measured as a qualitative variable, is associated with a 3–10% increased cancer risk (4)(5). Since BPE is a measurable variable on all breast MRIs, if it is shown to be predictive of future breast cancer risk, then BPE could be used to help stratify women to more or less frequent screening. Quantitative computer algorithm-based measurements of the enhancement of breast tissue could provide a more reproducible measure of BPE that is free of inter- and intra-reader variability which has been shown to be a notable limitation of the qualitative reader assessments (7). Such quantitative measures could potentially provide an even higher predictive accuracy of breast cancer risk. To date, no assessment of quantitative BPE features has been performed to determine their association with the risk of subsequent development of breast cancer in a high-risk population undergoing screening MRI. Some studies have examined automatic and semi-automatic measures of BPE in other contexts (8)(9)(10) with conflicting results. Furthermore, a majority of the studies that extracted quantitative features require defining a region of interest by reader(s) for the computation of BPE (11), making these features susceptible to interobserver variability. Therefore, the goal of this study is to automatically quantify the BPE in women undergoing high-risk screening MRI and determine the ability of these measurements to predict future breast cancer. Furthermore, the predictive power of these quantitative metrics will be compared to subjective BPE assessments made by multiple fellowship trained breast radiologists.

MATERIALS AND METHODS:

Patient Population

For this retrospective study, local institutional review board approval was secured and a waiver for informed consent was obtained. We identified all high-risk women (n=1039) who underwent screening breast MRI at our institution between August 1, 2004 and July 30, 2013. It is standard of practice at our institution for all pre-menopausal women to undergo high risk screening MRI during the second week of their menstrual cycle. Hormone replacement therapy was not an exclusion criterion as this is not always recorded in the MRI intake form, but anecdotally the use of hormone replacement therapy is extremely low (near 0%) in our patient population. Only MRIs with axial and bilateral breast images were eligible for inclusion. For these patients, the imaging and pathology reports were queried through July 30, 2015 to identify subsequent cancer diagnoses. The high-risk screening indication was noted. For each of the identified cancer patients (n=61) in the cohort, two control patients from the same patient pool were added by matching age and high-risk indication. Each selected control had at least two years of negative imaging follow up. After identifying a cohort of 183 high-risk patients, 50 patients were excluded due to missing T1 non-fat saturated sequences. The final cohort consisted of 133 high-risk patients including 46 cancer and 87 control patients. Please note the cohort of 183 patients was used in a previous study (reference redacted to preserve anonymity) where we evaluated the subjective assessment of BPE. In the present work, we are evaluating automatic (and thus 100% reproducible) BPE measures.

Image Data

For all patients, the following MR sequences (pulse sequence type: gradient echo) were used for data pre-processing and feature extraction: (1) a T1-weighted fat saturated pre-contrast sequence, (2) T1-weighted fat saturated first post contrast sequence, and (3) T1-weighted non-fat-saturated pre-contrast sequence. The MRI scanner details, image acquisition parameters, and contrast agents for these patients are shown in Table 1. . Images for the majority of patients in the cancer (48%) and control (58%) cohorts were acquired using 3T scanner from GE Healthcare (Little Chalfont, UK). For the majority of patients in both the cancer (85%) and control cohorts (92%), Magnevist (Bayer Healthcare, Berlin, Germany) was used as the contrast agent. All contrast agents were gadolinium-based and a weight-based (0.2 mL/kg) dosing protocol was used. The number of slices varied from (128–200), slice thickness varied from (1–1.3)mm, FOV values were within (26–40) cm, and spatial resolution were as follows: 512 × 512 (92/133), 448 × 448 (37/133), 384 × 384 (1/133), 320 ×320 (3/133).

Image Preprocessing

For each study, the pre-contrast fat saturated sequence was registered to the first post-contrast fat saturated sequence for further processing. This registered pre-contrast sequence and the first post-contrast sequence was used to calculate the subtracted sequence and the maximum intensity projection (MIP) image.

Mask Generation

To calculate BPE features, we first divided the breast MRI into different regions of interest. The regions included: (1) the breast region, (2) the fibroglandular tissue region, and (3) the heart region on the MIP. These regions were automatically segmented to obtain:

(a) a breast mask from the T1 non-fat saturated sequence

(b) a fibroglandular tissue (FGT) mask extracted from the T1 non-fat saturated sequence

(c) an FGT mask extracted from the fat saturated sequence

(d) a heart mask extracted from the MIP

The extraction processes of these masks are discussed next.

All image data pre-processing and mask extraction related tasks were conducted in MATLAB 2016b (The Mathworks, Natick, MA). The masks were extracted as follows:

(a) Breast mask generation: The breast mask segmentation using T1 fat saturated sequence was carried out as described in (12). This mask was registered to the first post contrast sequence. Both unregistered and registered breast masks were used to segment FGT as described below. The registered breast mask was used for feature extraction.

(b) FGT mask extraction from the T1 non-fat saturated sequence: The registered breast mask was overlapped with the first post contrast sequence and a fuzzy C-means clustering method (13) was applied to segment the fibroglandular tissue (FGT) mask. This FGT mask was used for feature extraction.

(c) FGT mask extraction from the T1 fat saturated sequence: The unregistered breast mask was overlapped T1 fat saturated sequence and a fuzzy C-means clustering method (13) was applied to segment the fibroglandular tissue (FGT) mask. This mask was registered to the first postcontrast sequence for further usage. This FGT mask was used for feature extraction.

(d) Heart mask extracted from the MIP: The maximum intensity values of the subtracted sequence were projected in z-direction to form the maximum intensity projection (MIP) image. The vessels on the MIP were identified by the BCOSFIRE algorithm (14) and additional post-processing consisted of image erosion to remove isolated voxels. The 2D breast mask on the MIP was generated by projecting the registered 3D breast mask on the MIP. Since we have two types of volumetric FGT masks, the FGT on the MIP was identified with the help of each of these volumetric FGT masks. The FGT masks in the MIP were finalized by removing the vessels. The chest cavity on the MIP was identified as the region outside the air and the 2D breast mask (obtained by projecting 3D registered breast mask). Finally, the heart mask was generated on the MIP by running an active contour segmentation (15) technique in the chest cavity.

Definition of Enhancement

Voxel enhancement is defined as a change in the intensity of the voxel in the first post-contrast image compared to that in the pre-contrast image. In our work, enhancement in MR volumes is quantified in terms of the percentage change in the intensity of the voxel in the first post-contrast image compared to the pre-contrast image. On the MIP, the enhancement is the relative difference in the intensity of the voxels. Normalized enhancement is defined as the enhancement of a voxel divided by the enhancement of the heart. For specific mathematical definitions of enhancement used in each of the measures of BPE please see the supplementary material.

Features of BPE Extracted in this Study

Eight BPE features were extracted using each of the two FGT masks. Four of these features were extracted using 3D MR volumes (pre-contrast, first post-contrast, and FGT mask) and the remaining four features were calculated from the MIP. The short descriptions of these eight features are as follows:

a. Vol_f1: This feature quantifies what percentage of FGT voxels in the entire breast enhances more than 100% in the first post-contrast sequence compared to the pre-contrast sequence.

b. Vol_f2: This feature quantifies the average enhancement of FGT voxels.

c. Vol_f3: The normalized enhancement of FGT is calculated. Next, a curve is generated such that each point on it indicates what proportion of FGT voxels have enhanced more than a threshold corresponding to that point. For example, in Fig. 1, the point (10, 0.48) indicates that 48% of the FGT voxels has a normalized enhancement of 10% or more. Area under the curve as expressed in Fig. 1 is the value of this feature.

d. Vol_f4: This feature is similar to Vol_f3 but the proportion of FGT is calculated over the total breast volume.

e. MIP_f1: This feature quantifies what proportion of the parenchyma enhances on the MIP.

f. MIP_f2: This feature quantifies the average value of the normalized enhancement of FGT on the MIP.

g. MIP_f3: This feature takes into account the proportion and intensity of BPE on the MIP by calculating the product of MIP_f1 and MIP_f2.

h. MIP_f4: This feature quantifies the normalized enhancement of the MIP by estimating the area under the curve on which each point is the proportion of normalized enhancement (y axis) exceeding a given threshold (x axis).

Further details about the features extracted can be found in the supplementary material. An example of enhanced FGT in MIP is shown in Fig. 2.

Subjective Assessment of BPE

Five breast radiologists (with 2, 10, 11, 17, and 24 years of post-fellowship experience) were included as readers in this study. The readers were blinded to the patient outcomes, the high-risk indication, the scanner selections and the contrast agents used. The studies were independently reviewed by each reader and the BPE (minimal, mild, moderate and marked) according to the 5th edition BI-RADS Atlas (16) was recorded. To record the BPE, the readers followed the description in BI-RADS that states that BPE "refers to both the volume of enhancement as well as the intensity of the enhancement and that an evaluation of BPE should take both into consideration". The BPE states of minimal, mild, moderate and marked were converted to ordinal variables by assigning 1, 2, 3 and 4. The primary measures evaluated in this study were mean and median BPE assessment across the five readers for each study. The inter-reader agreement was calculated using Fleiss Kappa.

Machine Learning-based Models using Computer-Extracted Features

Two multivariate logistic regression models (each using 8 computer-extracted BPE features) were constructed to predict the occurrence of cancer in the study population over a follow-up period of two years: (a) Machine learning model 1: BPE features were based on the FGT mask on the fat saturated sequence and (b) Machine learning model 2: BPE features were based on the FGT segmentation using the non-fat-saturated sequence.

Statistical Analysis

AUC and Confidence Interval—To evaluate the prognostic value (in terms of predicting the occurrence of cancer over a follow-up period of two years) of the breast parenchyma assessment conducted by readers as well as the machine learning models, we calculated the area under the receiver operating characteristics curve (AUC) using the *proc* package (17) in R (http://www.r-project.org/) using leave-one-out cross validation. The pooled AUCs from predicted scores of the trained models were calculated. The confidence intervals of the AUCs were estimated using the Delong's method (18).

Comparison of Subjective BPE and Predicted BPE—To compare the BPE features and readers' mean BPE values, we calculated the correlation between the individual feature values and readers' mean BPE values. To verify if the computer-extracted features were independently predictive of the development of breast cancer over a follow-up period of two years, we calculated the *p*-values from a bivariate logistic regression model (function *glm* in R) at 5% significance level. The dependent variable was the occurrence of cancer and for the independent variables, the predicted scores from the machine learning models as the first covariate and a measure of the subjective score (any of the individual reader's score, mean score, or median score) as the second covariate.

Computation of Odds Ratio: When calculating the odds ratio, we split the patients into two groups (one for low-risk of subsequent cancer and one for high-risk of subsequent cancer) in two different ways: (a) by discriminating minimal versus mild, moderate and marked patients using the median score of the readers and (b) by discriminating minimal and mild versus moderate and marked patients using the median score of the readers. We noted the proportion of patients present in each group for each split. For the average reader score

and the scores from the machine learning models, the patients were split according to the score predicted by the variable/model using a cut-off value that helps maintaining the relative proportions of the low-risk of subsequent cancer and high-risk of subsequent cancer groups the same as obtained using the median readers' score.

RESULTS

Characteristics of Study Population

The characteristics of the study population are shown in Table 2. Most subsequent cancers were invasive ductal carcinoma which were ER positive (61%), PR negative (53%), and HER2 negative (97%).

Performance of Imaging Features for Assessing Subsequent Development of Breast Cancer

The AUC of each feature to predict the occurrence of cancer is presented in Table 3. In general, the MIP based features have better individual AUCs than the volumetric features. One volumetric feature and two MIP based features have AUCs more than 0.62 using both types of FGT masks.

Comparison of Mean BPE from Readers and Imaging Features

The readers had fair average pairwise agreement (Fleiss Kappa κ=0.38, 95% CI: 0.34 – 0.42). The mean readers' score had a moderate average agreement (κ=0.57, 95% CI: 0.51 – 0.63) with all readers. All the quantitative features extracted from the images were positively correlated (Pearson's linear correlated coefficient ρ =0.27–0.67) with the mean readers' score. The highest correlation (ρ = 0.67) was demonstrated by MIP_f1, which is the proportion of parenchymal enhancement on the MIP, extracted using the first post-contrast sequence. The lowest correlation (ρ = 0.27) was found with MIP_f2, which is the mean value of the normalized enhanced FGT. The average values of correlation for volumetric features (0.52) and MIP based features (0.53) were similar.

The performances of the readers as well as computer models are shown in Table 4. Both of the models based on the automatically extracted features had better AUCs than mean and median subjective scores.

As obtained from the bivariate logistic regression models, the computer models (Machine learning model 1 and model 2) were predictive of subsequent cancer independently of the median score of readers ($p<0.025$ and $p<0.003$ respectively), mean score from readers ($p<0.025$ and $p<0.002$ respectively), and the scores from each individual reader (maximum of 5 *p*-values for model 1 <0.025 and maximum of 5 *p*-values for model 2 $p<0.0021$ respectively).

The odds ratio obtained using the subjective scores and the automatically extracted scores are shown in Table 5 based on two thresholds. The automatic imaging features performed better than the subjective features for all thresholds, having an odds ratio greater or equal to the mean and median reader scores.

DISCUSSION:

In this study of high-risk breast cancer patients undergoing screening MRI, we extracted automatic features of BPE. We found a statistically significant association between the risk of subsequent breast cancer and quantitative BPE features derived from three-dimensional images and two-dimensional projection images. Furthermore, the predictive performance of these quantitative BPE features was overall better than that achieved by the subjective BPE measurements from the human readers.

Out of the 8 features extracted, 3 features had AUC values higher than that obtained by the subjective scores for predicting cancer risk: Vol_f4, MIP_f2, and MIP_f4. For the volumetric features used in our study, Vol_f3 and Vol_f4 performed better than the other two volumetric features. Vol_f3 and Vol_f4 worked in a broader spectrum by considering multiple threshold levels (10 % to 100%) of enhancement with equal importance in their calculations, whereas Vol_f1 considered a single level (10%) of enhancement. Vol_f2 is the mean level of enhancement of the FGT voxels, and thus represented a single dominant level of enhancement despite considering all enhancement levels. The mean AUC of risk prediction using these individual volumetric features for the high-risk screening patients was 0.55 in our study, whereas using the MIP based features the mean individual AUC was 0.6. While MIP_f1 quantified the proportion of enhancement in the BPE on the MIP, it did not take into account the heart intensity on the MIP. However, the three remaining MIP based features used the heart intensity in their calculations. This indicates that while quantifying the MIP based BPE, the enhancement of the FGT relative to the heart is important.

Presently, BPE is defined by the subjective assessment of readers which is based on both the volume and intensity of enhancement(19). Among the features quantified in our study, MIP_f1 had the best correlation with the mean readers' BPE assessment. This feature is based on the proportion of parenchymal enhancement on the MIP images which suggests that readers are relying heavily on MIP images when determining BPE, despite no guidance from the BI-RADS Atlas. Interestingly, the MIP_f1 was one of the least predictive features for future breast cancer. This may also explain the limited predictive power of prior work that has utilized qualitative assessments of BPE, but which did not derive how readers made these assessments [4] [5] (20). In contrast, MIP_f2 had the worst correlation with the mean readers' BPE assessments, but it had the best performance for predicting future cancer. The MIP_f2 feature utilizes the mean value of the normalized enhanced FGT on the MIP images. If BPE measurements assessed by human readers are going to be of value in predicting future breast cancer, then the definition of BPE in the BI-RADS Atlas might need to be adjusted and readers should focus on the mean normalized enhancement rather than the proportion of enhancement in MIP. As normalized enhancement is not an intuitive measurement for radiologists, training will need to be developed to determine if radiologists can accurately reproduce this metric. Alternatively, since quantitative BPE features can be more precise and reproducible it may be best to move away from BPE assessments by human readers.

Our methodology of using quantitative features to predict future cancer builds upon the work of prior investigators who have applied similar methodologies but to different tasks.

Identifying quantitative features that correlate with reader BPE assessments has been evaluated by several authors (21) (22) (19). While Kajihara et al. (23) recorded the association of the menstrual cycle and semi-automatically extracted BPE feature that quantified the percentage enhancement of the most enhanced FGT region in the early and delayed phases of enhancement, we used the FGT from the entire breast to quantify the BPE. Response to both neoadjuvant chemotherapy therapy (24) and risk-reducing salpingo-oopherectomy surgery (10) have also been studied using BPE and our proportional FGT enhancement curves using multiple thresholds were formed based on the features they proposed. However, the areas (Vol_f3 and Vol_f4) under these curves were used as features instead of the individual points on these curves. A fully automated feature extraction technique (8) was used to quantify early, mid, and late BPE from the MRI volumes containing benign or cancerous lesions and shown to predict cancer risk in premenopausal and post-menopausal patients groups separately. In contrast, we specifically used a high-risk screening cohort with normal MRIs and extracted all the features using the early enhancement.

We used FGT masks from two different sequences: T1 non-fat saturated sequences and first post-contrast sequence. Features derived from the FGT mask using T1 non-fat saturated sequences, including most individual features and machine learning model 2, performed better than features based on FGT from the first post-contrast sequence as well as subjective scores which had access to all sequences. The FGT segmentation from the first post-contrast sequence can be influenced by the enhancement of the tissue as normal parenchyma enhances in early contrast enhanced MRI (25). However, FGT masks from T1-non-fat saturated sequences remain unaffected by enhancement which might explain in part the better performance of the features based on T1-non-fat saturated sequence-based masks. We found that the effect of mask was (a) more prominent in the multivariate model compared to the univariate models and (b) more prominent in volumetric features (9% variation) and MIP based features (3% variation).

The MRI sequences included in our study were from multiple scanners, and different magnetic field strengths were used for their acquisition. The range of the data acquired spans a decade. Different contrast agents were used to acquire the images, though one of the contrast agents was used for the majority of the scans. Thus, our results were robust to the variability in the dataset. However, future studies can be conducted on datasets having uniform protocols to find if better performance of the algorithm can be obtained as several FGT enhancement features were found to be stable (26) under varying scanning protocols.

Our study has limitations. The extracted imaging features used the first post contrast image of the screening MRI as the only post-contrast sequence. In the future, more features can be extracted from the delayed sequences to study their effect on the prediction of future breast cancer risk. However, our features showed associations with the subsequent development of breast cancer. Moreover, our study is single institutional and retrospective in nature. A multi-institutional study needs to be done to assess the association of automatic features with the subsequent development of cancer, followed by the evaluation of these features in an independent test set. However, our preliminary results are based on a dataset that has patient data spanning over a decade with considerable variability. Finally, for extensive validation to

determine if this study can have a broad clinical appeal, further investigation needs to be conducted in a prospective setting.

In conclusion, we demonstrated that a multivariate model comprising automatically extracted features of BPE from volumetric and two-dimensional projection images from screening MRI in high-risk patients can be associated with future breast cancer risk. Further validation needs to be conducted in a multi-institutional large-scale setting to assess the robustness and translational value of these features in a clinical setting.

Supplementary Material

Refer to Web version on PubMed Central for supplementary material.

Abbreviations:

MRI	Magnetic resonance imaging
BPE	Background parenchymal enhancement
FGT	Fibroglandular tissue
MIP	Maximum intensity projection
AUC	Area under receiver operating characteristics curve

REFERENCES:

1. Siegel RL, Miller KD, Jemal A: Cancer statistics, 2016. CA Cancer J Clin 2016; 66:7–30. [PubMed: 26742998]
2. Smith RA, Brooks D, Cokkinides V, Saslow D, Brawley OW: Cancer screening in the United States, 2013. CA Cancer J Clin 2013; 63:87–105.
3. Bae MS, Sung JS, Han W, et al.: Survival outcomes of screening with breast MRI in high-risk women. J Clin Oncol 2017; 35(15_suppl):1508.
4. Dontchos BN, Rahbar H, Partridge SC, et al.: Are Qualitative Assessments of Background Parenchymal Enhancement, Amount of Fibroglandular Tissue on MR Images, and Mammographic Density Associated with Breast Cancer Risk? Radiology 2015; 276:371–380. [PubMed: 25965809]
5. King V, Brooks JD, Bernstein JL, Reiner AS, Pike MC, Morris EA: Background parenchymal enhancement at breast MR imaging and breast cancer risk. Radiology 2011; 260:50–60. [PubMed: 21493794]
6. Müller-Schimpfle M, Ohmenhaüser K, Stoll P, Dietz K, Claussen CD: Menstrual cycle and age: influence on parenchymal contrast medium enhancement in MR imaging of the breast. Radiology 1997; 203:145–149. [PubMed: 9122383]
7. Saha A, Harowicz MR, Mazurowski MA: Breast cancer MRI radiomics: An overview of algorithmic features and impact of inter-reader variability in annotating tumors. Med Phys 2018; 0.
8. Hu X, Jiang L, Li Q, Gu Y: Quantitative assessment of background parenchymal enhancement in breast magnetic resonance images predicts the risk of breast cancer. Oncotarget 2017; 8:10620–10627. [PubMed: 27895314]
9. Bennani-Baiti B, Dietzel M, Baltzer PA: MRI Background Parenchymal Enhancement Is Not Associated with Breast Cancer. PLoS One 2016; 11:e0158573. [PubMed: 27379395]
10. Wu S, Weinstein SP, DeLeo MJ, et al.: Quantitative assessment of background parenchymal enhancement in breast MRI predicts response to risk-reducing salpingo-oophorectomy:

preliminary evaluation in a cohort of BRCA1/2 mutation carriers. Breast Cancer Res 2015; 17:1. [PubMed: 25567532]

11. Bignotti B, Signori A, Valdora F, et al.: Evaluation of background parenchymal enhancement on breast MRI: a systematic review. Br J Radiol 2016; 90:20160542. [PubMed: 27925480]
12. Mazurowski MA, Grimm LJ, Zhang J, et al.: Recurrence-free survival in breast cancer is associated with MRI tumor enhancement dynamics quantified using computer algorithms. Eur J Radiol 2015; In Press.
13. Bezdek JC: Pattern Recognition with Fuzzy Objective Function Algorithms. Norwell, MA, USA: Kluwer Academic Publishers; 1981.
14. Fraz MM, Rudnicka AR, Owen CG, Barman SA: Delineation of blood vessels in pediatric retinal images using decision trees-based ensemble classification. Int J Comput Assist Radiol Surg 2014; 9:795–811. [PubMed: 24366332]
15. Chan TF, Vese LA: Active contours without edges. IEEE Trans image Process 2001; 10:266–277. [PubMed: 18249617]
16. D'Orsi CJ, Radiology AC of, Committee B-R: ACR BI-RADS Atlas: Breast Imaging Reporting and Data System. 2013.
17. Robin X, Turck N, Hainard A, et al.: pROC: an open-source package for R and S+ to analyze and compare ROC curves. BMC Bioinformatics 2011; 12:77. [PubMed: 21414208]
18. DeLong ER, DeLong DM, Clarke-Pearson DL: Comparing the areas under two or more correlated receiver operating characteristic curves: a nonparametric approach. Biometrics 1988:837–845. [PubMed: 3203132]
19. Tagliafico A, Bignotti B, Tagliafico G, Tosto S, Signori A, Calabrese M: Quantitative evaluation of background parenchymal enhancement (BPE) on breast MRI. A feasibility study with a semi-automatic and automatic software compared to observer-based scores. Br J Radiol 2015; 88:20150417. [PubMed: 26462852]
20. Telegrafo M, Rella L, Stabile Ianora AA, Angelelli G, Moschetta M: Breast MRI background parenchymal enhancement (BPE) correlates with the risk of breast cancer. Magn Reson Imaging 2016; 34:173–176. [PubMed: 26597834]
21. Ha R, Mema E, Guo X, et al.: Three-Dimensional Quantitative Validation of Breast Magnetic Resonance Imaging Background Parenchymal Enhancement Assessments. Curr Probl Diagn Radiol 2016; 45:297–303. [PubMed: 27039221]
22. Jansen SA, Lin VC, Giger ML, Li H, Karczmar GS, Newstead GM: Normal parenchymal enhancement patterns in women undergoing MR screening of the breast. Eur Radiol 2011; 21:1374–1382. [PubMed: 21327872]
23. KAJIHARA M, GOTO M, HIRAYAMA Y, et al.: Effect of the Menstrual Cycle on Background Parenchymal Enhancement in Breast MR Imaging. Magn Reson Med Sci 2013; 12:39–45. [PubMed: 23474960]
24. Chen JH, Yu HJ, Hsu C, Mehta RS, Carpenter PM, Su MY: Background Parenchymal Enhancement of the Contralateral Normal Breast: Association with Tumor Response in Breast Cancer Patients Receiving Neoadjuvant Chemotherapy. Transl Oncol 2015; 8:204–209. [PubMed: 26055178]
25. Kuhl CK, Schild HH: Dynamic image interpretation of MRI of the breast. J Magn Reson Imaging 2000; 12:965–974. [PubMed: 11105038]
26. Saha A, Yu X, Sahoo D, Mazurowski MA: Effects of MRI scanner parameters on breast cancer radiomics. Expert Syst Appl 2017; 87:384–391. [PubMed: 30319179]

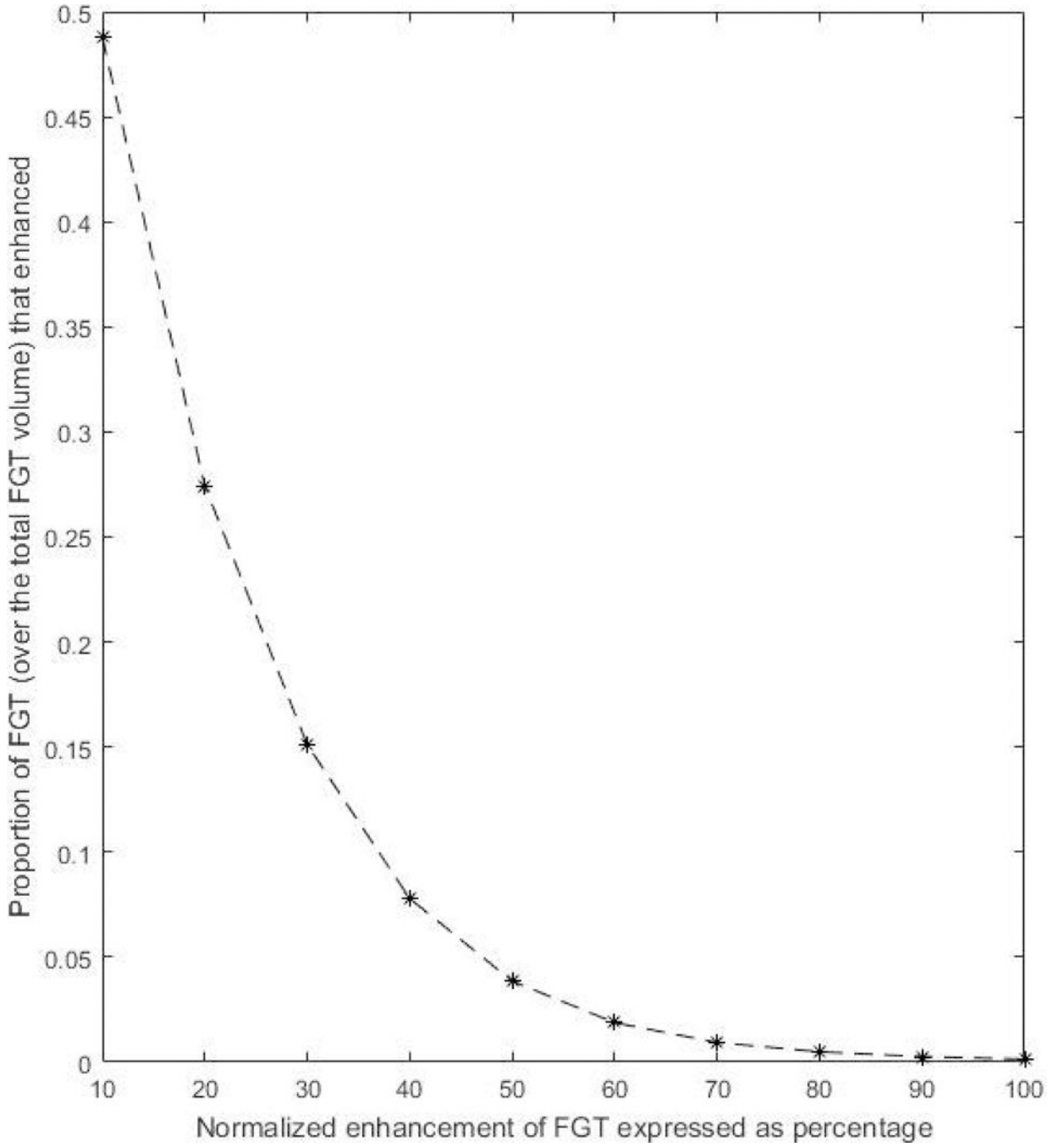

Figure 1.

A curve showing the proportion of FGT voxels (over the total FGT volume) that has a normalized enhancement of T% or more. T ranges from 10 to 100 with intervals of 10.

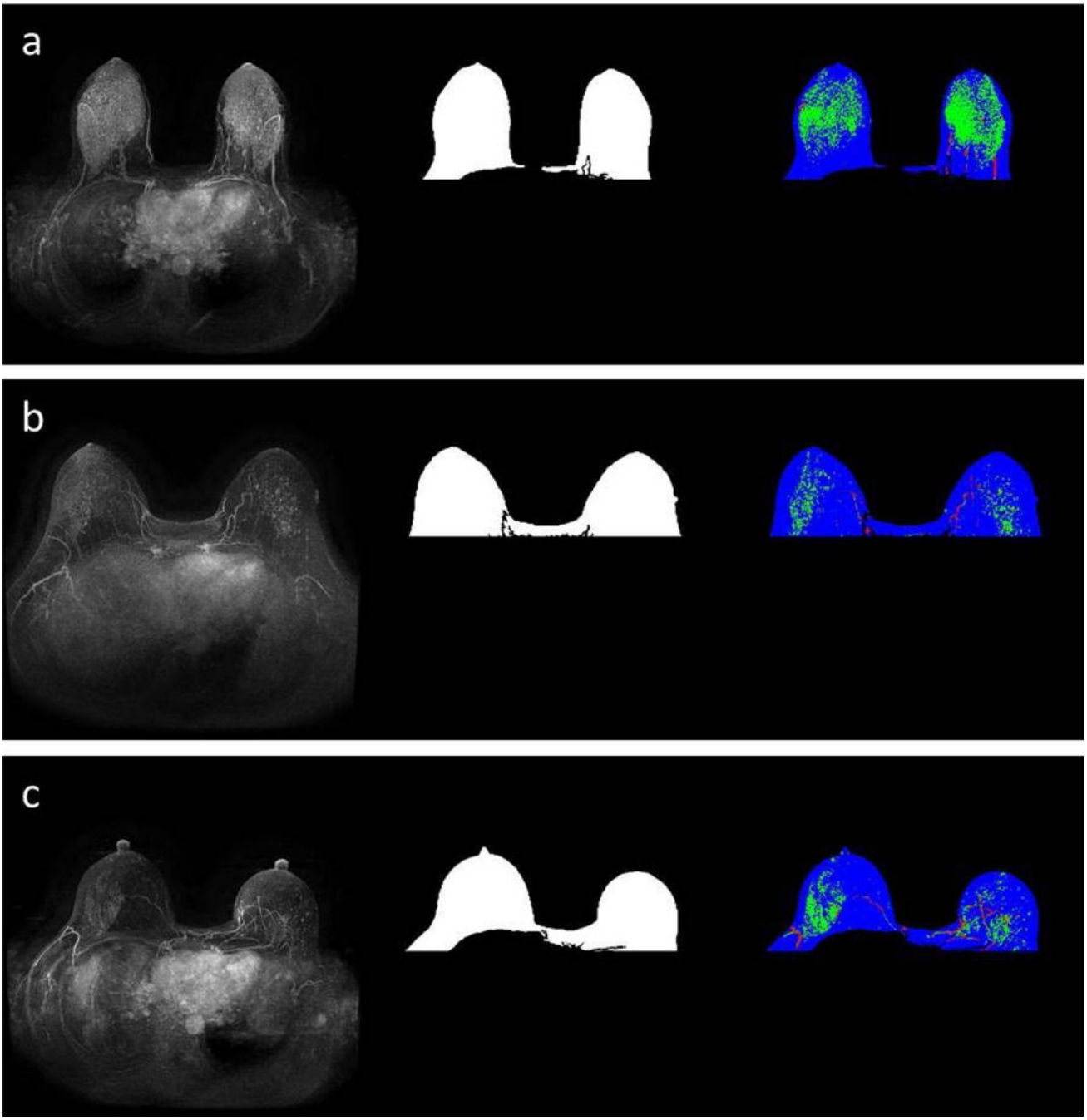

Figure 2.

Images from a patient that subsequently developed cancer (a) and the two matched controls (b and c respectively). The MIPs are presented in the first column and the breast masks are shown in the second column. The third column represented enhanced FGT on the MIP in green, vessels in red and remaining breast mask in blue. The FGT for these images was extracted from the corresponding T1 non-fat saturated sequence.

Table 1:

MRI protocols in Cancer and Control Patients

Scanner Parameter	Details	Model	TR (ms)	TE(ms)	Contrast Agent Type (Count)	Subsequent Cancer Count N (%)	Control Count (%)
Manufacturer	GE Healthcare, Little Chalfont, UK	Signa HDx	4.88–6.76	2.27–2.54	Magnevist (64)	21 (46)	43 (49)
		Signa HDxt	4.88–6.10	2.28–2.74	Magnevist (26), Multihance (2)	5 (11)	23 (26)
	Siemens, Munich, Germany	MAGNETOM TrioTim	3.54– 4.09	1.36–1.58	Magnevist (14), Multihance (2), Unknown (5)	8 (17)	13 (15)
		MAGNETOM Avanto	4.12–4.54	1.27–1.51	Magnevist (14), Multihance (3), Gadavist (1)	10 (22)	8 (9)
		MAGNETOM Trio	3.54	1.4	Unknown(1)	1 (2)	0 (0)
		MAGNETOM Espree	4	1.33	Magnevist (1)	1 (2)	0 (0)
Magnetic Field Strength	1.5T	MAGNETOM Avanto	4.12–4.54	1.27–1.51	Magnevist (14), Multihance (3), Gadavist (1)	10 (22)	8 (9)
		Signa HDxt	4.88–4.98	2.28–2.36	Magnevist (9)	3 (7)	6 (7)
		Signa HDx	4.88–5.08	2.27–2.41	Magnevist (11)	1 (2)	10 (11)
		MAGNETOM Espree,	4	1.33	Magnevist (1)	1 (2)	0 (0)
	3.0T	Signa HDx	5.11–6.76	2.35–2.54	Magnevist (53)	20 (43)	33 (38)
		Signa HDxt	5.07–6.10	2.33–2.74	Magnevist (17), Multihance(2)	2 (4)	17 (20)
		MAGNETOM Trio Tim	3.54– 4.09	1.36–1.58	Magnevist (14), Multihance (2), Unknown (5)	8 (17)	13 (15)
		MAGNETOM Trio	3.54	1.4	Unknown(1)	1 (2)	0 (0)

Table 2

Patient demographics in the cancer and control cohorts

	Cancer cohort N (%), mean (range)	Control cohort N (%), mean (range)
	(n=46)	(n=87)
Age at index MRI (years)	50.3 (27.4–73.9)	50.1 (28.4–75.9)
Race/ethnicity		
White or Caucasian	37 (80)	71 (82)
Black or African American	7 (15)	10 (11)
Other or not reported	2 (5)	6 (7)
Follow up duration (years)	2 (0 –5.1)	4.5 (2.1 – 6.7)
Subsequent cancer diagnosis		
DCIS	13 (28)	NA
Invasive lobular carcinoma	3 (7)	NA
Invasive ductal carcinoma	30 (65)	NA

Table 3

AUCs for individual features

FGT mask source	Vol_f1	Vol_f2	Vol_f3	Vol_f4	MIP_f1	MIP_f2	MIP_f3	MIP_f4
First post-contrast sequence	0.47	0.43	0.60	0.64	0.49	0.66	0.60	0.64
T1 non- fat -saturated sequence	0.48	0.46	0.66	0.63	0.50	0.66	0.60	0.66

Table 4

AUC values from different variables for predicting risk of occurrence of cancer

Name of the variable	AUC (95% confidence interval)
Mean reader scores	0.59 (0.49–0.70)
Median reader scores	0.60 (0.51–0.69)
Machine learning model 1	0.63 (0.52 – 0.73)
Machine learning model 2	0.70 (0.60 – 0.79)

Table 5

Odds ratios for the subjective scores and automatic imaging features

Threshold used according to median score of readers to categorize patients into low and high BPE	Odds Ratio for mean reader score	Odds Ratio for median reader score	Odds Ratio for using features from first-postcontrast Based FGT mask	Odds Ratio for using features from first-T1 non-fat-saturated Based FGT mask
minimal vs mild, moderate, and marked	2.44	2.66	2	4.21
minimal and mild vs moderate and marked	0.78	0.85	2.41	3.1